Trends and Outlook of Computational Chemistry and Microkinetic Modeling for Catalytic Synthesis of Methanol and DME

Jongmin Park [1,†] , Hyo Seok Kim [1,†], Won Bo Lee [1,*] and Myung-June Park [2,3,*]

[1] School of Chemical and Biological Engineering, Seoul National University, Seoul 08826, Korea; parkjm10@snu.ac.kr (J.P.); snukhs@snu.ac.kr (H.S.K.)
[2] Department of Chemical Engineering, Ajou University, Suwon 16499, Korea
[3] Department of Energy Systems Research, Ajou University, Suwon 16499, Korea
* Correspondence: wblee@snu.ac.kr (W.B.L.); mjpark@ajou.ac.kr (M.-J.P.); Tel.: +82-2-880-7076 (W.B.L.); +82-31-219-2383 (M.-J.P.)
† These authors equally contributed.

check for updates

Abstract: The first-principle modeling of heterogeneous catalysts is a revolutionarily approach, as the electronic structure of a catalyst is closely related to its reactivity on the surface with reactant molecules. In the past, detailed reaction mechanisms could not be understood, however, computational chemistry has made it possible to analyze a specific elementary reaction of a reaction system. Microkinetic modeling is a powerful tool for investigating elementary reactions and reaction mechanisms for kinetics. Using a microkinetic model, the dominant pathways and rate-determining steps can be elucidated among the competitive reactions, and the effects of operating conditions on the reaction mechanisms can be determined. Therefore, the combination of computational chemistry and microkinetic modeling can significantly improve computational catalysis research. In this study, we reviewed the trends and outlook of this combination technique as applied to the catalytic synthesis of methanol (MeOH) and dimethyl ether (DME), whose detailed mechanisms are still controversial. Although the scope is limited to the catalytic synthesis of limited species, this study is expected to provide a foundation for future works in the field of catalysis research based on computational catalysis.

Keywords: computational chemistry; microkinetic modeling; methanol synthesis; DME synthesis
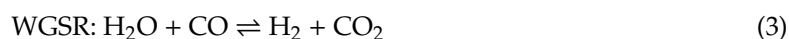
1. Introduction

First-principle modeling is a combination of solid state physics and surface chemistry [1]. It can be used to find the electronic structure of a catalyst, which relates to its reactivity on the surface, where the bonds of reactant molecules break to form new bonds. Using a computational catalyst is a paradigm shift approach in contrast to the trial and error method that has been used for decades [2], as it can rapidly replace conventional experimental tools, including infrared (IR), X-ray diffraction (XRD), and Raman spectra. Previously, detailed reaction mechanisms were hard to completely understand because the reaction networks are very complex and little was known about their physicochemical exactness [3]. However, the first-principle approach makes it possible to analyze a specific elementary reaction of a reaction system, thereby shedding light on the reaction mechanisms of many catalytic systems.

The use of a microkinetic analysis on catalytic reaction systems originated from Bush and Dyer's work [4], where they conducted an experimental and computational analysis of complex kinetics for industrial high-temperature chlorocarbon rearrangement and hydrocarbon cracking by evaluating the surface reaction mechanisms to predict the performance of the industrial reactors.

Since then, several researchers have considered the detailed catalytic reaction mechanisms in kinetic modeling [5,6]. Dumesic et al. established the framework microkinetics of heterogeneous catalysis [7]. As a microkinetic model includes all possible elementary steps, a rigorous investigation of the detailed reaction pathways is possible. Further, the dominant pathway can be elucidated through a microkinetic model, which could be increasingly helpful in designing catalysts and improving the catalytic process by deepening our understanding regarding the fundamentals of reaction mechanisms. Therefore, the combination of a quantum chemical approach and microkinetic modeling can create synergetic effects that facilitate the analysis of catalytic reaction mechanisms.

As global warming worsens and fossil fuels are depleted, the utilization of carbon dioxide (CO_2), which is one of the main contributors to greenhouse gases, has become of great interest to researchers [8–12]. The electroreduction of CO_2 to low-molecular-weight organic chemicals has been one of the most well-known CO_2 utilization techniques for over a century [13–15]. The conversion of CO_2 to methanol (MeOH) and dimethyl ether (DME) is a promising CO_2 utilization method because the products are renewable, economically competitive, and eco-friendly fuels [16,17]. MeOH and DME can be applied in various capacities, including internal combustion engines [18], solvents, refrigerants, and propellants. Both MeOH and DME are being widely synthesized in many industries, and there have been many studies on their synthesis, ranging from the development of catalysts and their kinetics to process systems engineering. However, the kinetics and detailed mechanisms are still controversial, leaving several questions unsolved. For example, which pathway is dominant between CO and CO_2 hydrogenations, and how does catalyst support affect reactivity [19,20]. For these reasons, there is a need for further investigation to enhance and improve the MeOH and DME production processes.

MeOH synthesis from syngas has three overall reactions, including CO and CO_2 hydrogenations and the water–gas shift reaction (WGSR):

$$\text{CO hydrogenation: } CO + 2H_2 \rightleftharpoons CH_3OH \tag{1}$$

$$\text{CO}_2 \text{ hydrogenation: } CO_2 + 3H_2 \rightleftharpoons CH_3OH + H_2O \tag{2}$$

$$\text{WGSR: } H_2O + CO \rightleftharpoons H_2 + CO_2 \tag{3}$$

Meanwhile, DME synthesis from MeOH occurs by one overall reaction, as follows:

$$\text{MeOH dehydration: } 2CH_3OH \rightleftharpoons CH_3OCH_3 + H_2O \tag{4}$$
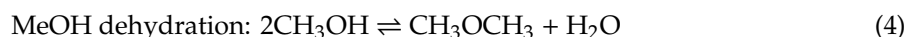
In general, the dehydration of MeOH over solid acid catalysts is known to occur in the two competitive pathways—the associative (direct) and dissociative (sequential) pathways—as illustrated in Figure 1. However, there is still controversy regarding which pathway is dominant over the other. On the associative pathway, two MeOH molecules adsorb to the catalyst, and the MeOH hydration proceeds to form water and DME at the same time. Meanwhile, on the dissociative pathway, two MeOH molecules are adsorbed one by one to produce water (water elimination or formation reaction) by the first MeOH molecule, followed by the production of DME by the second molecule (DME elimination or formation reaction).
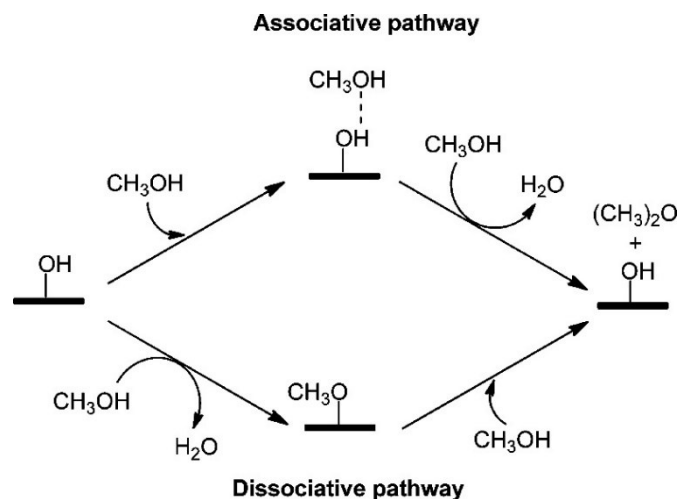
Figure 1. The associative and dissociative pathways of methanol (MeOH) dehydration. Reprinted with permission from [21]. Copyright (2015) American Chemistry Society.

2. Results and Discussion

2.1. Computational Chemistry

2.1.1. Methanol Synthesis over Cu-based Catalysts

Cu-based catalysts are well known for their involvement in MeOH synthesis from syngas. Despite various experimental studies regarding MeOH synthesis, since the appearance of the first commercial MeOH synthesis plant by BASF Inc. in 1923, some of their detailed mechanism is still unknown [22]. Early-stage theoretical modeling of MeOH synthesis was reported in the 1990s [23,24], where vibrational frequencies for hydrogenation intermediates were successfully predicted and compared to FT-IR experimental results. Since then, researchers have been trying to elucidate a deeper understanding of the MeOH synthesis reaction on Cu-based catalysts. Bauschlicher et al. calculated the binding energy and vibrational frequencies of CO on a Cu(100) surface using a 38 atom cluster model [25] and found that the binding energy of CO was dependent on the cluster size, while the vibrational frequency was not.

The accuracy of the density functional theory (DFT) calculations in MeOH synthesis over Cu catalysts was reported [26] by calculating the reaction Gibbs energies with three exchange-correlation (XC) functionals: Perdew–Burke–Ernzerhof (PBE), Heyd–Scuseria–Ernzerhof (HSE), and random phase approximation (RPA). Interestingly, each XC functional created different results, where PBE was shown to be the best, followed by HSE. Wellendorff et al. [27] suggested a new XC functional, the Bayesian error estimation functional with van der Waals correlation (BEEF-vdW), which is the only XC functional that describes the kinetics and selectivity of MeOH synthesis concerning CO and CO_2. BEEF-vdW was compared to revised PBE (RPBE) on the Cu(211) surface by calculating the Gibbs free energy diagrams using both XC functionals [28]. It was shown that the CO_2 hydrogenation pathway with the BEEF-vdW functional was consistent with the previous experimental results.

A major challenge in the field of catalysis is the difficulty of identifying active sites and their thermodynamics. While there are many reports on the active sites of industrial $Cu/ZnO/Al_2O_3$ catalysts [24,29–31], the debate about the effectiveness of these sites is ongoing because the reactivity of the CO and CO_2 hydrogenations over metal catalysts is highly correlated with their oxide supports (Figure 2). Behrens et al. [30] suggest that the active site on Cu/ZnO-based catalysts is the stepped Cu(211) surface with Zn alloying. Comparative DFT calculations on three different surfaces were conducted and the Gibbs free energies of each reaction path were calculated. The results indicated that the reaction intermediates, such as HCO, H_2CO, H_3CO, were more stably absorbed on the stepped Cu(211). Furthermore, the active site was stabilized by the ZnO support, thereby increasing the

fractional surface area of Cu(211) with the ZnO concentration. However, researchers still question whether there exists a difference in reactivity between the ZnCu alloy and the ZnO/Cu catalyst. In Kattel et al.'s DFT calculation [32], it was shown that the ZnCu(211) surface was oxidized when the lattice Zn was transformed into ZnO, and the oxidized site enhanced the MeOH production.
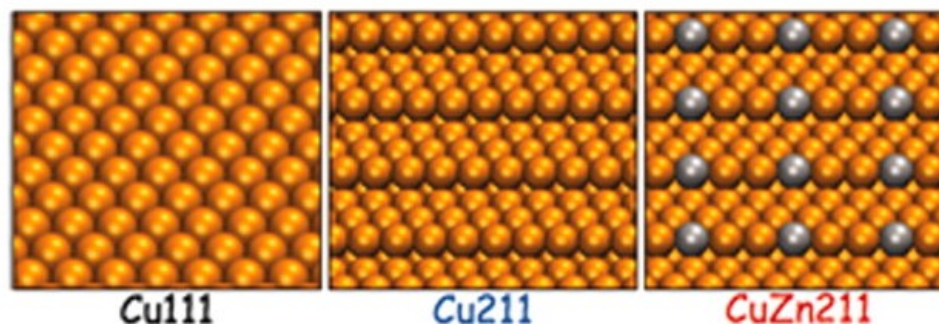

Figure 2. Density functional theory (DFT) calculation models for each catalyst facet. Reprinted with permission from [30]. Copyright (2012) American Association for the Advancement of Science.

Subsequently, researchers investigated if the same effect could be found for supports other than ZnO. Reichenbach et al. [29] performed rigorous DFT calculations on ZnO/Cu systems to investigate the effect of ceria and zirconia supports on Cu. The accuracy of the reaction energies and activation energy calculated by DFT-PBE was verified by the coupled-cluster method (CCSD(T)) and experimental data. When the bond lengths and Wannier orbitals of the intermediates and adsorbates were calculated, shown in Figure 3, the main reaction pathway of the ZnO support was different from that of zirconia and ceria. This is because the absorbed configurations of Zr and Ce were more stable than those without supports.
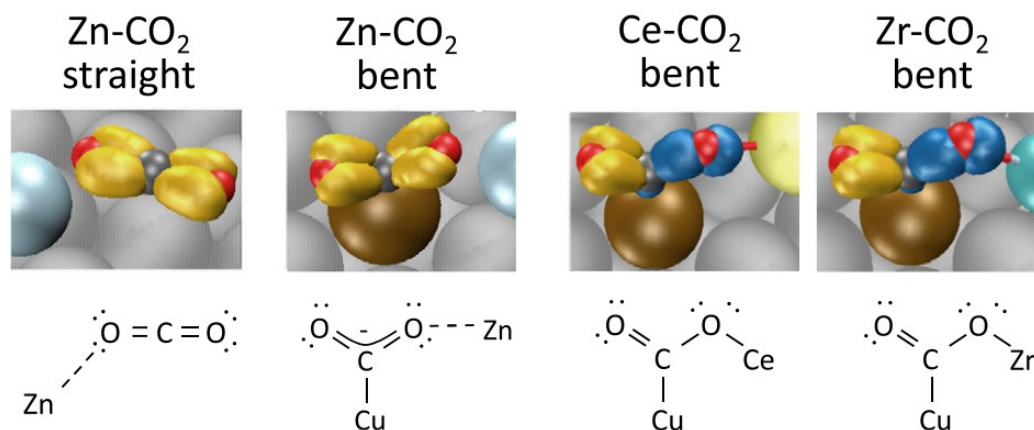

Figure 3. Wannier orbitals of $[CO_2]^-$, $[HCOO]^-$ (formate), HCOOH (formic acid), and CO_2 bound straight to Zn, bent to Zn, Ce, and Zr in the surface model. Reprinted with permission from [29]. Copyright (2018) Elsevier.

Our knowledge of elementary reactions has been expanded with microkinetic modeling research, thereby ending the long-lasting debate on reaction mechanisms. One of the applicative examples is the effect of water in the reaction mechanism, and more specifically, whether the water molecule itself or the dissociated O*/OH* species join the reaction. A DFT calculation clearly showed that the presence of water molecules influences the reaction pathway by changing both the thermodynamically and kinetically preferred intermediates. It was also shown that the coverage of O*/OH* species on the Cu surface could promote the formation of MeOH [33].

Very recently, a practical first-principle microkinetic model was suggested, where all reaction rates are calculated using the DFT for activation energies and fitting reaction pre-factors to experimental

data [34]. The reactivity of Cu alloys, including the commercial-like catalyst and three others, was calculated [35] based on the suggested elementary reactions and microkinetic modeling. Consequently, the superior performance of the commercial catalyst was shown to make great contributions in understanding the reaction and development processes efficiently.

2.1.2. Methanol Synthesis over Other Catalysts

The first-principle calculation made it possible to evaluate the reactivity and reaction mechanism of promising catalytic materials, among which ceria attracted great attention [36]. Ceria is known to have two reaction pathways: (1) The COOH pathway via a carboxyl intermediate and (2) the HCOO pathway via a formate intermediate. This first-principle microkinetic modeling showed that the HCOO pathway is kinetically more favored.

Experimental values of the formation energies of MeOH synthesis on Cu, Ru, Rh, Pd, Ag, Re, Os, Pt, and Au surfaces were used to validate the reactivity of the Cu cation and suggest other promising metal catalysts [37]. Although this report is the first attempt to screen catalysts using computational chemistry on MeOH synthesis, it did not consider the adsorption site of metal surfaces, which is critical in determining the reactivity of catalysts. Additionally, the reaction mechanism was simple, and reaction barriers were not calculated.

2.1.3. First-Principle Modeling on DME Synthesis

For the DME synthesis, hydrophobic zeolites are well known for their high catalytic selectivity and reactivity. Zeolite is composed of cages, pores, and channels of various sizes, and its reactivity and selectivity are dependent on the relative size between the components of zeolite and reactant molecules. The structural database of whole zeolites is well established in the International Zeolite Association database [38]. As zeolite is widely used for the synthesis of olefin, gasoline, and DME, a considerable amount of research on zeolite catalysis has been performed to understand its properties [2,39,40]. This section reviews the zeolite structure, Brønsted acid site, MeOH adsorption reaction, and MeOH to DME reaction pathway, with a focus on DME synthesis.

A Brønsted acid site of Al-substituted zeolite is commonly accepted to initiate MeOH adsorption, followed by its dehydrogenation reaction. In 1995, Haase et al. [41] succeeded in calculating the interaction of MeOH with a Brønsted acid site of a simple zeolite structure using the second-order Moller–Plesset perturbation theory (MP2) (Figure 4). Their calculations showed a reasonable match to the experimental results. They also observed that the OH stretching frequency of MeOH changed due to the electronic correlation with the acid site of the catalyst, which is consistent with the IR spectroscopy results.
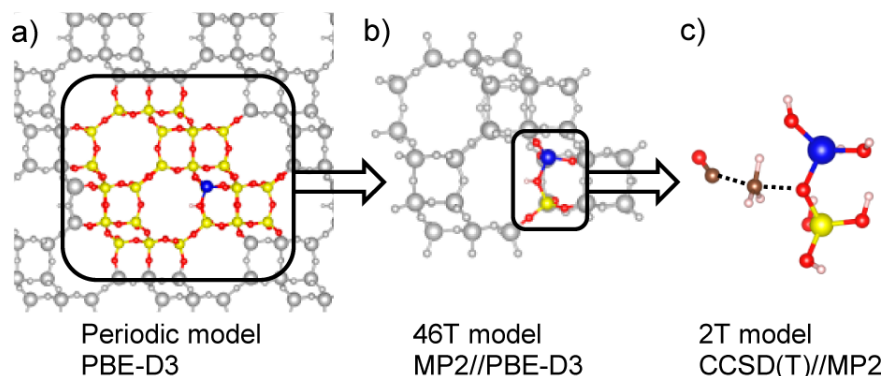

Figure 4. Models of a high silica zeolite with the chabazite (CHA) topology (H-SSZ-13); (**a**) periodic model with DFT Perdew–Burke–Ernzerhof (PBE)-D3 method, (**b**) 46 atomic cluster model with Møller–Plesset perturbation theory (MP2)/PBE-D3 method, and (**c**) 2T cluster model with coupled-cluster method (CCSD)(T)/MP2 method, where T abbreviates the SiO_4 tetrahedron, which is a basic unit of zeolites. Reprinted with permission from [41]. Copyright (2017) American Chemical Society.

Recently, Plessow et al. [42] calculated the H-SSZ-13 zeolite using a hierarchical cluster approach to secure an acceptable level of accuracy, which could provide a detailed mechanism of the MeOH dehydrogenation reaction. They performed quantum chemical calculations at different levels in different models to ensure the accuracy of their results. Their work is the first reported to accurately calculate the transition states and activation energy of the MeOH dehydrogenation reaction, which is significant, not only for MeOH to DME, but also for MeOH to olefin reactions.

2.2. Microkinetic Modeling

2.2.1. Methanol Synthesis over Cu-based Catalysts

ZnO was deemed appropriate as a catalyst for MeOH synthesis in the 1920s, even though it required harsh operating conditions (T = 600–700 K and P = 200–300 bar) [43,44]. It was not until after the 1960s that a MeOH synthesis process that used Cu-based catalysts, which operates at low pressures, was developed. Since then, MeOH has been synthesized industrially from syngas over a $Cu/ZnO/Al_2O_3$ catalyst [45], and several studies using microkinetic models have been conducted to elucidate the reaction mechanisms. In 1992, Taylor et al. [46] synthesized surface formate experimentally by using a mixture of CO_2 and H_2 over a clean Cu(100) surface and used a microkinetic model to propose a pathway for formate synthesis that was composed of only three elementary steps (CO_2 and H_2 adsorption steps and a surface reaction between the adsorbed CO_2* and H*). They determined that the surface reaction was the rate-limiting step by comparing the rates of the other reactions and the binding energies, and calculated the kinetic parameters from the experiments. In 1995, a microkinetic model for all the MeOH synthesis pathways, including the 16 elementary steps for the CO_2 hydrogenation and the WGSR, was suggested by Askgaard et al. [47]. The hydrogenation of H_2COO* to methoxy (H_3CO*) and oxide (O*) intermediates was assumed as the rate-limiting step based on the Cu(100) single-crystal experiments of Rasmussen et al. [48]. The parameters were estimated from the gaseous phase thermodynamic data, as well as by surface science studies. In 1997, a dynamic microkinetic model for CO_2 hydrogenation and the WGSR with 13 elementary steps over Cu/ZnO catalysts was proposed [49], reflecting the transient changes in particle shape observed by in situ extended X-ray absorption fine structure (EXAFS) and XRD/EXAFS [50–52]. This model considered the dynamic changes in the concentration of oxygen vacancies at the Zn–O–Cu interfaces, and, as a result, provided a better description than the static microkinetic model. Grabow and Mavrikakis [20] presented a comprehensive mean-field microkinetic model for MeOH synthesis in 2011, including CO and CO_2 hydrogenations, and WGSRs as the overall reactions, as well as 49 elementary steps for those reactions. In particular, the overall WGSR was divided into two pathways, the redox and carboxyl, as described in Table 1.

Table 1. Redox and carboxyl pathways for the water–gas shift reaction (WGSR). Reprinted with permission from [53]. Copyright (2008) American Chemical Society.

Redox Pathway	Carboxyl Pathway
$CO + * \rightleftharpoons CO$*	
$H_2O + * \rightleftharpoons H_2O$*	
$H_2O* + * \rightleftharpoons H* + OH$*	
$OH* + * \rightleftharpoons O* + H$*	$CO* + OH* \rightleftharpoons COOH* + $*
$2OH* \rightleftharpoons H_2O* + O$*	$COOH* + * \rightleftharpoons CO_2* + H$*
$CO* + O* \rightleftharpoons CO_2* + $*	$COOH* + OH* \rightleftharpoons CO_2* + H_2O$*
$CO_2* \rightleftharpoons CO_2 + $*	
$2H* \rightleftharpoons H_2 + 2$*	

Furthermore, the novel surface intermediates, such as HCOOH* and CH_3O_2*, and gaseous phase byproducts, such as formic acid (HCOOH), formaldehyde (CH_2O), and methyl formate ($HCOOCH_3$), were considered. A large amount of the DFT calculations were performed with the assumption that

the Cu(111) surface was used for the binding energies and vibrational frequencies of the gaseous phase and adsorbed species, and the activation energies of all the surface reactions. The results were applied to the microkinetic model, which indicated that the carboxyl pathway was the dominant pathway in the WGSR, and both the CO and CO_2 hydrogenations contributed to the MeOH synthesis. The hydrogenation of a methoxy intermediate (CH_3O^*) was the common rate-limiting step for CO and CO_2 hydrogenation, while $HCO^* + H^* \rightleftharpoons CH_2O^* + ^*$ and $HCOOH^* + H^* \rightleftharpoons CH_3O_2^* + ^*$ were relatively slow steps in the CO and CO_2 hydrogenations, respectively. These results show that partially oxidized Cu surfaces, such as Cu(110), Cu(100), and Cu(211), might be more appropriate models than Cu(111) for MeOH synthesis over a commercial $Cu/ZnO/Al_2O_3$ catalyst. In 2012, Peter et al. [54] adapted the microkinetic model of Ovesen et al. [49], in which the sensitivity of the structure with several low-index Cu surfaces, including Cu(111), Cu(110), and Cu(100), was studied in the interest of comparing the microkinetic model with the power law and Langmuir–Hinshelwood–Hougen–Watson (LHHW) models.

Rubert-Nason et al. [55] proposed some advanced solution methods for microkinetic models and applied them to MeOH synthesis over a Cu-based catalyst in 2014. They reformulated a typical microkinetic model, consisting of a system of ordinary differential equations, to a system of nonlinear equations through careful scaling and binding with 16 elementary steps that were the subset of the 49 elementary steps considered in Grabow and Mavrikakis's work [20]. As a result, the computational burden for solving the model was reduced, which allowed for better results of the parameter estimation to fit the experimental data, owing to a more systematic and comprehensive search of the parameter space.

In 2015, Tang et al. [56] investigated the effects of the Cu/ZnO interface on MeOH synthesis via CO_2 hydrogenation based on a combination of the DFT + U calculations to account for the strong electron correlations in the ZnO support. The catalyst model considered in their microkinetic model is described in Figure 5.
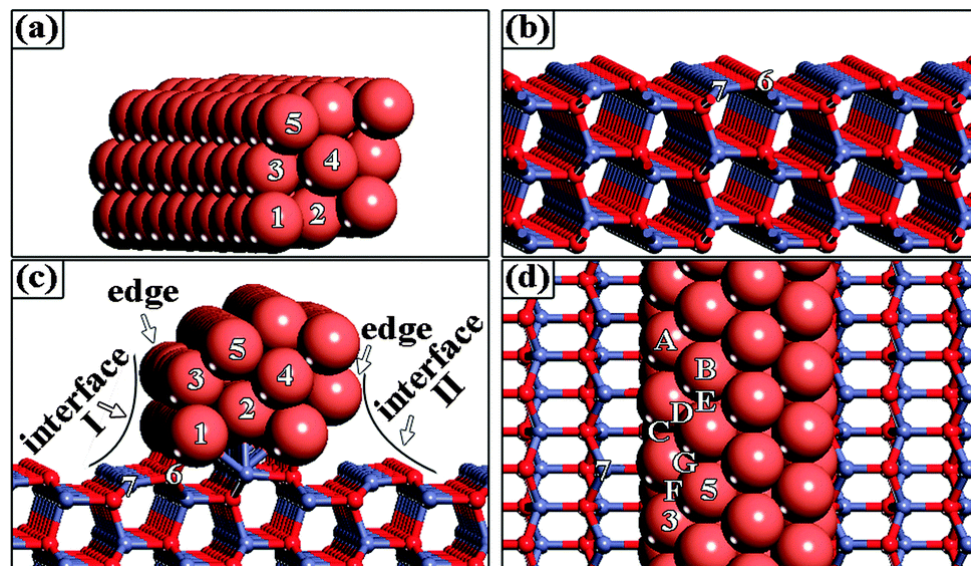

Figure 5. Catalyst model for the DFT + U calculations; an isolated (**a**) Cu(111) strip, (**b**) ZnO($10\bar{1}0$), (**c**) side and (**d**) top views of the Cu/ZnO catalyst model. Reprinted with permission from [56]. Copyright (2015) Royal Society of Chemistry.

A total of 38 elementary steps at the Cu site of the Cu/ZnO interface were considered, including the HCOO, COOH, and CO pathways, the diffusion of H* from the interface to the bulk Cu(111) surface or the ZnO, and vice versa. Based on the turnover frequency calculations, the MeOH synthesis at the Cu site of the interface was shown to be negligible, as a result of the weak interaction of CO_2 with the interfacial Cu site, and no byproducts, including CO, CH_2O, and HCOOH, were produced. Therefore,

they concluded that the bulk Cu(111) surface was the active site, and the spillover of H* produced at the Cu site of the interface onto the bulk Cu(111) promoted CO_2 hydrogenation. Meanwhile, Janse van Rensburg et al. [57] presented a microkinetic analysis for CO and CO_2 hydrogenations over Cu(111), Cu(211), and Zn-modified Cu (CuZn)(211) surfaces. DFT-based Gibbs free energy data for the 11 elementary steps were extracted from previous studies [28,30] and an in-house developed code [58] was used for the microkinetic analysis. They concluded that the Cu(111) had the lowest reactivity, while Cu(211) and CuZn(211) had similar reactivities. Note that the reactivity of Cu(211) was higher than that of CuZn(211) for isolated CO_2 hydrogenation, while CuZn(211) showed a higher reactivity for both isolated CO hydrogenation and combined CO and CO_2 hydrogenation. In 2018, Tameh et al. [26] conducted microkinetic modeling for CO and CO_2 hydrogenations on the Cu(211) surface to compare three XC functionals: PBE, HSE hybrid, and RPA functionals. The quasi-equilibrium assumption was applied to the adsorption and desorption reactions for the calculation of the site fractions of gaseous species. A total of 14 elementary steps were considered for isolated CO hydrogenation, isolated CO_2 hydrogenation, and combined CO and CO_2 hydrogenation. The ode15s solver of MATLAB$^®$ (MathWorks Inc.) was used to determine the stiff ordinary differential equations. They suggested that $HCO^* + H^* \rightleftharpoons H_2CO^* + {}^*$ and $HCOOH^* + H^* \rightleftharpoons H_2COOH^* + {}^*$ were the rate-limiting steps for CO and CO_2 hydrogenation, respectively. Additionally, they determined that CO hydrogenation predominated CO_2 hydrogenation for each functional, although the difference of the overall barrier between CO and CO_2 hydrogenation depended on the functionals. Furthermore, different functionals led to different results for the most abundant surface intermediates. Xu et al. [33] investigated the role of water in CO_2 hydrogenation on the Cu(211) surface by combining DFT and microkinetic studies, where the research focus was to determine if MeOH synthesis was promoted by a water molecule or O/OH derived from water. They found that the existence of O/OH played an important role, and the MeOH synthesis rate was increased by destabilizing the formate intermediate (the site fraction of HCOO* was decreased) and lowering the activation barriers. The CatMAP software package [59,60], a Python module for descriptor-based microkinetic mapping, developed by the Nørskov group, was used to conduct their microkinetic analysis.

Furthermore, microkinetic modeling was conducted in our previous study [34], where the computational burden was alleviated by combining DFT calculations with the unity bond index-quadratic exponential (UBI-QEP) method. Thus, the adsorption energies for 28 elementary steps of the CO and CO_2 hydrogenations and the WGSR were calculated from the DFT calculations, and then the UBI-QEP method was used for the activation energies by utilizing our calculated adsorption energies. The pre-exponential factors were estimated by fitting the experimental data, which also reduced the computational costs and ensured the reliability of the model. In the microkinetic model, the formate intermediate was considered as a bidentate species, and the hydrogenation of a methoxy intermediate ($CH_3O^* + H^* \rightleftharpoons CH_3OH^*$) was proposed as the common rate-limiting step of both the CO and CO_2 hydrogenations.

2.2.2. MeOH Synthesis over Other Catalysts

There have also been microkinetic studies that consider different kinds of catalysts for MeOH synthesis to find the most effective catalysts, among which Ga_2O_3 as a promoter [61] or the bulk support [62,63] of finely dispersed Pd gained attention for CO_2 conversion to MeOH. Chiavassa et al. [64] developed a microkinetic model for MeOH synthesis from a CO_2/H_2 mixture over Ga_2O_3–Pd/silica catalysts in 2009, including a total 12 elementary steps for the CO and CO_2 hydrogenations, and the WGSR. In this model, the surfaces of both Ga and Pd, and Pd–Ga interfaces were identified as the active sites, and the migration and diffusion of the adsorbed hydrogen to the Pd–Ga_2O_3 interface and the Ga phase, respectively, were also included in the reaction mechanism. This model suggested that the competitive mechanism was the more plausible route than the uncompetitive one, and the hydrogenation of the formate intermediates and their decomposition on the Ga surface were proposed to be the rate-limiting steps. In 2014, Medford et al. [44] analyzed the thermochemistry and reaction

network for MeOH synthesis over a Zn-terminated ZnO(0001) catalyst using the DFT and a steady-state microkinetic model. A total of 19 elementary steps were considered, and the kinetic parameters were obtained based on DFT calculations. Here, the rate-limiting steps were suggested to be $CH_2O^* + H^* \rightleftharpoons CH_3O^* + ^*$ under industrial conditions and $CH_3O^* + H^* \rightleftharpoons CH_3OH^* + ^*$ at high temperature and low pressure conditions. In the same year, Ye et al. [65] conducted a combined DFT and microkinetic study for MeOH synthesis from CO_2 hydrogenation over a Pd_4/In_2O_3 catalyst, in which a Pd_4 cluster was placed on the $In_2O_3(110)$ surface, and the reaction network for three possible pathways of CO_2 hydrogenation, consisting of 28 elementary steps, was considered, as shown in Figure 6. As there exist significant varieties and complexities in the detailed catalytic reaction pathways in the literature, the elementary steps that have been widely used are provided in Figure 6, where CO_2 was firstly hydrogenated by the HCOO or reverse water-gas shift (RWGS) pathway, forming mono-HCOO or trans-COOH, respectively, and each could produce HCOOH. H_2CO was hydrogenated by the competitive reactions to produce H_3CO or H_2COH, and both intermediates were converted to MeOH. Among the HCOO, HCOOH, and RWGS, DFT calculations show that the HCOOH pathway was unfavorable due to its high activation energy and the HCOO pathway was dominant compared to the RWGS. It was shown by the microkinetic model that $H_2COO^* + H^* \rightleftharpoons H_2CO^* + OH^*$ and cis-$COOH^* + H^* \rightleftharpoons CO^* + H_2O^*$ were the rate-limiting steps of the HCOO and RWGS pathways, respectively. The activated H^* on the Pd cluster and H_2O on the In_2O_3 promoted the HCOO pathway by lowering the activation energy of the rate-limiting step.
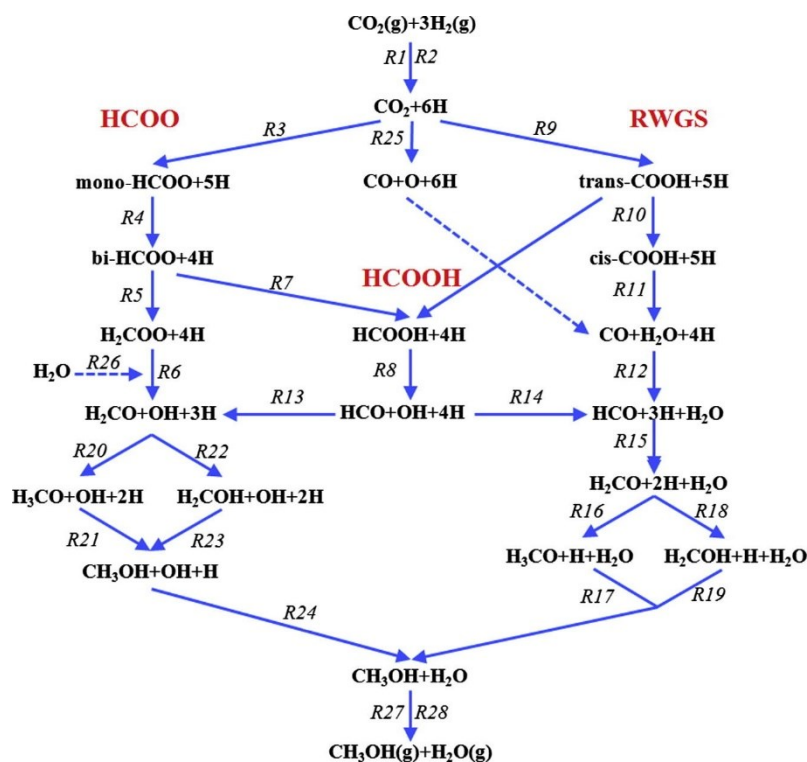

Figure 6. Three possible pathways of CO_2 hydrogenation. Reprinted with permission from [65]. Copyright (2014) Elsevier.

In 2016, Cheng and Lo [36] studied the mechanisms of CO_2 hydrogenation over a reduced ceria(110) catalyst. The HCOO and COOH pathways were identified with 21 elementary steps, while dispersion interactions were assumed negligible in the DFT calculations of adsorption energies. The activation energies were calculated by applying the climbing image nudged elastic band (CI-NEB) method [66] and the Brønsted–Evans–Polanyi (BEP) relation [67–69], and the pre-exponential factors were obtained by calculating the vibrational frequencies and partition functions. A formaldehyde

intermediate (CH$_2$O*) was the key intermediate, and the HCOO pathway was dominant. Furthermore, the rate-limiting step was the conversion of H-formalin (H$_2$COOH*) to CH$_2$O*. In 2017, Huš et al. [35] conducted the first RWGS (the same as the COOH pathway mentioned above) pathway, which consisted of network-principle multiscale modeling and experiments to investigate the mechanisms of CO$_2$ hydrogenation over Cu-based catalysts, including Zn$_3$O$_3$/Cu, Cr$_3$O$_3$/Cu, Fe$_3$O$_3$/Cu, and Mg$_3$O$_3$/Cu. For the catalyst model, M$_3$O$_3$ (M = Zn, Mg, Fe, Cr) was doped on the Cu(111) surface, as described in Figure 7. The active sites consisted of Cu and the interface of Cu–M with the equal ratio, and 33 elementary steps were considered, including the HCOO and COOH pathways and H* diffusion. Both the pre-exponential factors and activation energies were calculated from the DFT, and all elementary reaction rates were scaled by a factor of 10^{-3} to guarantee model stability and reduce computational costs. Kinetic Monte Carlo simulations (kMC) were also conducted for more detailed results to conclude that the HCOO pathway predominated the four Cu-based catalysts, even though the catalytic performances were different for each catalyst.
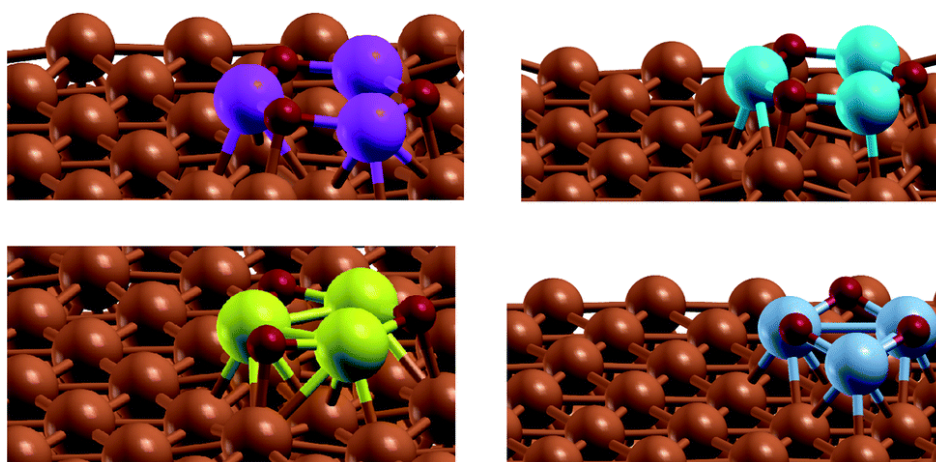

Figure 7. Catalyst models of M$_3$O$_3$-doped Cu. Reprinted with permission from [35]. Copyright (2017) Royal Society of Chemistry.

In 2018, Frei et al. [70] conducted microkinetic simulations based on their DFT results for CO$_2$ hydrogenation and the WGSR on the In$_2$O$_3$(111) surface. By solving the microkinetic model based on a differential reactor model under steady-state conditions using Maple^{TM} (Maplesoft), the apparent activation energies and reaction orders were determined. They then expanded their study in 2019 to In$_2$O$_3$ promotion by Pd [71], in which the microkinetic modeling methods were similar to their former work. Compared with the pure In$_2$O$_3$ catalysts, the apparent activation energies for MeOH synthesis were lower when the Pd atoms were doped.

The PdIn intermetallic catalyst was recently proposed for CO$_2$ hydrogenation owing to its high activity, selectivity, and stability [72]. Wu and Yang [73] conducted mechanistic studies for CO$_2$ hydrogenation and CO formation with 24 elementary steps by combining the DFT and microkinetic analysis on the intermetallic PdIn catalyst, as described in Figure 8. The CatMAP module was used for the microkinetic analysis, and the dominant pathway was determined to be HCOO* → HCOOH* → H$_2$COOH* → CH$_2$O* + OH* → CH$_3$O* + OH* → CH$_3$OH (g) + H$_2$O (g). The dominant pathway for CO formation depended on the type of surface; CO$_2$* → CO* + O* and CO$_2$* → COOH* → CO* + OH* were preferred on PdIn(110) and (211), respectively. Furthermore, HCOOH* + H* → H$_2$COOH* was the rate-limiting step on PdIn(110), while on PdIn(211), it changed from H$_2$COOH* → CH$_2$O* + OH* to HCOOH* + H* → H$_2$COOH* as a result of the temperature increase.
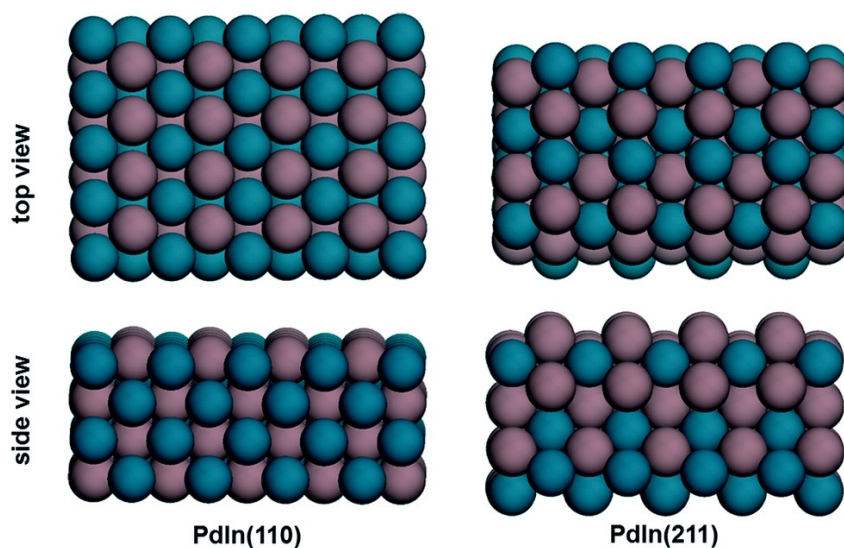
Figure 8. Surface models of PdIn(110) and PdIn(211); the Pd and In atoms are colored in blue and brown, respectively. Reprinted with permission from [73]. Copyright (2019) Royal Society of Chemistry.

The history of microkinetic studies on MeOH synthesis is summarized in Tables 2 and 3.

Table 2. Previous microkinetic studies for MeOH synthesis on Cu-Zn-Al (CZA) catalysts.

Researcher	Year	Reaction [§]	# of Steps	Catalyst Model	Kinetic Parameter	Rate-Limiting Step	Dominant Pathway [§]
Askgaard et al. [47]	1995	CO_2, WGS	16	Cu(100)	Estimation	Assumed	None
Ovesen et al. [49]	1997	CO_2, WGS	13	Cu(100), Cu(110), Cu(111)	Calculation with partition functions, estimation	Assumed	None
Grabow and Mavrikakis [20]	2011	CO, CO_2, WGS	49	Cu(111)	DFT, estimation	$H_3CO^* + H^* \rightarrow CH_3OH^* + ^*$	CO (1/3) and CO_2 (2/3)
Tang et al. [56]	2015	CO_2, WGS	38	Cu(111)/ZnO($10\bar{1}0$)	DFT + U	None	None
Janse Van Rensburg et al. [57]	2015	CO, CO_2	11	Cu(111), Cu(211), CuZn(211)	DFT	CO_2 hydrogenation: HCOOH (g) + $H^* \rightarrow$ $H_2COOH^* + ^*$ CO hydrogenation: $HCO^* +$ $H^* \rightarrow H_2CO^* + ^*$	CO
Tameh et al. [26]	2018	CO, CO_2	14	Cu(211)	DFT	CO_2 hydrogenation: $HCOOH^* + H^* \rightarrow H_2COOH^*$ $+ ^*$	CO_2
Xu et al. [33]	2019	CO_2	7	Cu(211)	DFT	None	None
Park et al. [34]	2019	CO, CO_2, WGS	28	Cu(111)	DFT, UBI-QEP, estimation	$H_3CO^* + H^* \rightarrow CH_3OH^* + ^*$	None

[§] CO, CO_2, and WGS represent the CO and CO_2 hydrogenations, and water–gas shift reaction, respectively.

Table 3. Previous microkinetic studies for MeOH synthesis on various catalysts.

Researcher	Year	Reaction [§]	# of step	Catalyst Model	Kinetic Parameter	Rate-Limiting Step	Dominant Pathway [§]
Chiavassa et al. [64]	2009	CO, CO_2, WGS	12	Ga_2O_3-Pd/silica	Estimation	$HCOO^* + H^* \rightarrow H_2COO^* + ^*$	None
Medford et al. [44]	2014	CO, CO_2, WGS	19	ZnO(0001)	DFT	Industrial condition: H_2CO^* $+ H^* \rightarrow H_3CO^* + ^*$High T and low P: $H_3CO^* + H^* \rightarrow$ $CH_3OH^* + ^*$	CO
Ye et al. [65]	2014	CO_2	28	Pd_4/In_2O_3	DFT	$H_2COO^* + H^* \rightarrow H_2CO^* +$ OH^*	HCOO pathway of CO_2
Cheng and Lo [36]	2016	CO_2	21	CeO_2(110)	DFT, BEP relation	$H_2COO^* + H^* \rightarrow H_2CO^* +$ OH^*	HCOO pathway of CO_2
Huš et al. [35]	2017	CO_2	33	Zn_3O_3/Cu, Mg_3O_3/Cu, Cr_3O_3/Cu, Fe_3O_3/Cu,	DFT	None	HCOO pathway of CO_2

Researcher	Year	Reaction [§]	# of step	Catalyst Model	Kinetic Parameter	Rate-Limiting Step	Dominant Pathway [§]
Frei et al. [70]	2018	CO_2, WGS	26	In_2O_3(111)	DFT	None	None
Frei et al. [71]	2019	CO_2, WGS	19	Pd-promoted In_2O_3	DFT	None	None
Wu and Yang [73]	2019	CO_2, WGS	24	PdIn(110), PdIn(211)	DFT	PdIn(110) and (211) at high T: $HCOOH^* + H^* \rightarrow H_2COOH^* + ^*$ PdIn(211) at low T: $H_2COOH^* + ^* \rightarrow H_2CO^* + OH^*$	HCOOH pathway of CO_2

[§] CO, CO_2, and WGS represent the CO and CO_2 hydrogenations, and water–gas shift reaction, respectively.

2.2.3. DME Synthesis

There have been few microkinetic studies that consider DME synthesis by MeOH dehydration. In 2011, Carr et al. [74] conducted DFT-based microkinetic modeling for MeOH dehydration over tungsten Keggin polyoxometalate (POM) clusters to evaluate the effects of acid strength on the dehydration rate. The elementary reaction schemes considered are shown in Figure 9. They applied the pseudo-steady-state hypothesis (PSSH) to all the adsorbed intermediates, the quasi-equilibrium assumption to MeOH adsorption, and the irreversibility assumption to the water and DME formation reactions to develop the kinetic equations. The most abundant intermediates on the catalyst were assumed, with methoxides and MeOH monomers for the dissociative pathway, and MeOH monomers and protonated dimers for the associative pathway. They concluded that the associative pathway was dominant under the tungsten Keggin POM clusters.
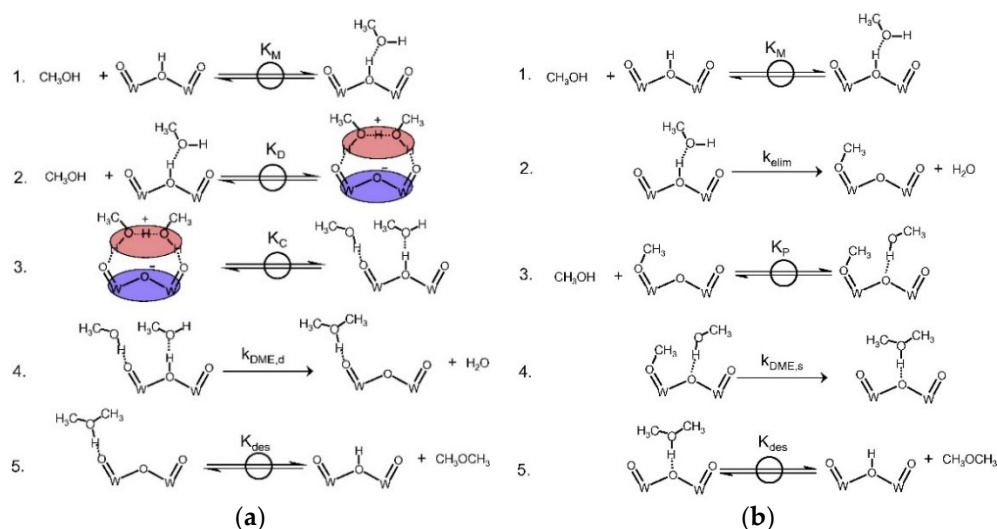

(**a**)   (**b**)

Figure 9. Elementary steps of MeOH dehydration on tungsten Keggin polyoxometalate (POM) clusters considered in [74]. (**a**) The associative pathway and (**b**) the dissociative pathway. Reprinted with permission from [74]. Copyright (2011) Elsevier.

In 2013, Moses and Nørskov [75] conducted periodic DFT calculations for MeOH dehydration over ZSM-22 to investigate the pathway dominancy by deriving the kinetic equations and calculating the relative reaction rates, in a similar process to Carr et al. [74] The quasi-equilibrium and irreversible step approximations were applied, and site fractions of the intermediates on non-acid sites were assumed to be negligible. Their results showed that the dissociative pathway was dominant, which is in opposition to the results of Carr et al. Although water lowered the activation energies of the key reactions, the overall reaction rate of the DME synthesis was barely influenced as a result of the entropy loss by the adsorption of water molecules. Furthermore, Moses and Nørskov concluded that acidity had nothing to do with the dominancy of the dissociative pathway. Jones and Iglesia [76] utilized a DFT and a microkinetic model to compare the associative and dissociative pathways in 2014. Periodic DFT

calculations with the van der Waals density functional (vdW-DF2) were conducted to simulate H-MFI zeolite [77]. The kinetic models were derived by applying the PSSH for the adsorbed intermediates and assuming the elementary steps to be quasi-equilibrated, except for the water and DME formation reactions, and specifying that the MeOH dimers were the most abundant adsorbed intermediates based on their IR spectra results. The conclusion was made that the associative pathway was dominant at T < 503 K and P = 0.1 bar or T < 570 K and P = 1 bar, while the dissociative pathway became dominant at higher temperatures and lower pressures. These results were explained by the enthalpy–entropy trade-off point of view.

In our recent study [78], a combination of the MP2 and microkinetic modeling was conducted for DME synthesis from MeOH over an H-zeolite catalyst. The MP2 was used instead of the DFT to consider the dispersion interactions, and nine elementary steps, including both the associative and dissociative pathways, were included to find the dominant pathway. The pre-exponential factors were estimated by fitting the experimental data. As a result, the dissociative pathway was determined to be dominant, and the DME formation reaction of the pathway was the rate-limiting step.

The history of microkinetic studies on DME synthesis is summarized in Table 4.

Table 4. Previous microkinetic studies on DME synthesis.

Researcher	Year	Catalyst Model	Kinetic Parameter	Rate-Limiting Step	Dominant Pathway
Carr et al. [74]	2011	Tungsten Keggin POM cluster	DFT	None	Associative pathway
Moses and Nørskov [75]	2013	ZSM-22	DFT	DME formation step of the dissociative pathway	Dissociative pathway
Jones and Iglesia [76]	2014	H-MFI	DFT	None	Dependent on T and P
Park et al. [78]	2020	H-zeolite cluster	MP2, Estimation	DME formation step of the dissociative pathway	Dissociative pathway

3. Methods

3.1. Computational Chemistry

This section examines the theory of computational chemistry for the catalytic research field, including the theories and calculation methods for calculating adsorption energy, vibrational frequency, and activation energy, to understand the properties of a catalyst, based on the DFT [79]. The field of DFT has become a starting point for the full-fledged application of computational chemistry and is currently used in various fields.

3.1.1. Surface Modeling

For modeling a catalytic reaction, it is essential to build an adequate surface model. The surface model has been developed in various ways along with its purpose. There are three surface models categorized by Sabbe et al. [80], which are a cluster model, embedded cluster model, and periodic model. The cluster model is a model that focuses on the active site, and has the advantage of being able to perform efficient calculations with few resources. However, it is difficult to simulate a complex catalyst surface because it cannot consider long-range interactions, such as electrostatic potential. The embedded cluster model makes up for the cluster model by introducing a simple model for long-range interactions. In the embedded cluster model, a short-range near the active site is calculated by the quantum mechanical approach, and the others are considered as a kind of perturbation. This approach effectively simulates the catalytic reaction, such as CO_2 reduction reactions [81]. The periodic slab model can be calculated for an infinitely regular surface that does not consider edges so that an accurate electronic structure for the crystal structure can be obtained. However, to simulate a surface with irregularities, such as defects or impurities on the surface, a supercell is required, which increases the computational cost.

3.1.2. Adsorption Energy

Adsorption energy is an important property used to investigate the catalytic reaction as it quantifies the amount or intensity of adsorption when the reactants in the gaseous phase adsorb onto the catalyst surface. The adsorption energy can be determined by calculating the ground state energies before and after adsorption using the DFT calculation and the difference between them, as follows:

$$E_{ads} = E_{slab \, + \, adsorbate} - (E_{slab} + E_{adsorbate}) \tag{5}$$

Early DFT calculations were only marginally able to predict the adsorption energy. Therefore, Feibelman et al. [82] constructed a model for CO adsorption on a Pt(111) catalyst to find the calculated adsorption energies using several XC functionals based on a generalized gradient approximation (GGA), such as Perdew–Wang 91 (PW91), PBE and RPBE, and overestimated experimental values. In the 2000s, Kresse et al. [83] introduced the semilocal functional to accurately calculate the adsorption energy of CO on Pt(111) to compensate for the underestimated value of the gap between the highest occupied molecular orbital (HOMO) and the lowest unoccupied molecular orbital (LUMO). They also demonstrated that the interaction between metal and the $2\pi^*$ orbital was overestimated in conventional DFT calculations, and suggested many alternative correction methods, including DFT + U, which is a hybrid functional [84,85]. The adsorption energy of many catalytic reactions has been calculated for various metal catalysts other than Pt, and a high consistency between experimental results and calculations has been accomplished. This method was also successfully applied to strongly correlated materials, such as NiO [86], as well as other materials [87].

3.1.3. Activation Energy

An important property in a catalytic reaction is the activation energy. Activation energy, which has been estimated experimentally in the form of the Arrhenius equation, can be calculated directly using computational chemistry. As activation energy is defined as the difference in energy between a transition state and the initial state, the geometry of the energy of both states must be obtained by the DFT.

The most widely known method for directly obtaining the transition state is the nudged elastic band (NEB) method [66,88], where the minimum energy path (MEP) between the states before and after the reaction on the potential energy surface are explored (Figure 10). A series of atomic configurations between the initial and final states are used for finding the MEP. These configurations describe the reaction pathway and are connected by spring forces in which the distance between configurations are fixed. Thus, the direction of the net force on a configuration is the sum of three forces: the spring force connected neighbor configuration, the perpendicular force induced by the potential energy surface, and the unprojected forces. Through iteration, each configuration moves to the nearest saddle point, and the MEP is found.
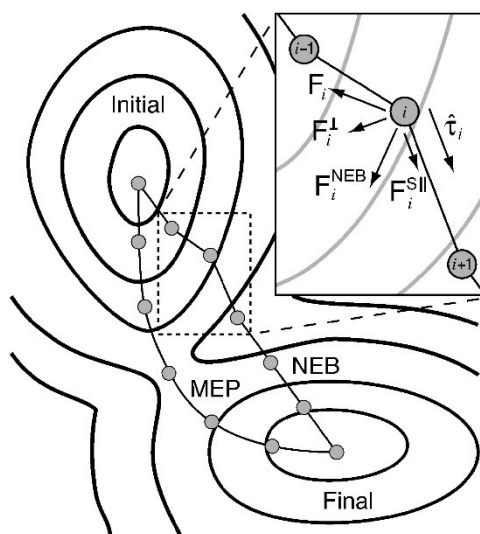
Figure 10. Illustration of the nudged elastic band (NEB) method on a potential energy surface (PES); F_i^{NEB}: nudged elastic band force, $F_i^{S\|}$: spring force along the tangential τ_i, $F_i^\perp$: perpendicular force, and F_i: the other forces. Reprinted with permission from [26]. Copyright (2000) AIP Publishing.

3.2. Microkinetic Modeling

Although closed-form empirical kinetic models, such as the power law and LHHW models, have been used widely [89,90] due to their relatively simple structure and appropriate fitness to experimental data, their limitations in describing changes in the rate-limiting steps under varying operating conditions, as well as the irrelevant parameters to the physical significance, have motivated the application of the microkinetic modeling approach, which considers detailed reaction mechanisms. To develop a microkinetic model, the overall reactions are divided into several elementary steps. For example, the overall reaction of CO_2 hydrogenation (Equation 2) is separated into the following elementary steps, based on the possible reaction pathways, in Table 5. CO_2 hydrogenation can occur via two pathways (COOH and HCOO pathways), which include eight elementary steps, while the adsorption and desorption of CO and CH_3OH, respectively, are the common steps in both pathways. Using a microkinetic model to augment the two competitive pathways, the role of each step is evaluated and the dominant pathway is elucidated.

Table 5. CO_2 hydrogenation mechanisms; this table was reproduced from [36].

COOH Pathway	HCOO Pathway
$CO_2 + * \rightleftharpoons CO_2*$	
$CO_2* + H* \rightleftharpoons COOH* + *$	$CO_2* + H* \rightleftharpoons HCOO* + *$
$COOH* + * \rightleftharpoons CO* + OH*$	$HCOO* + H* \rightleftharpoons H_2CO_2* + *$
$CO* + H* \rightleftharpoons HCO* + *$	$H_2CO_2* + H* \rightleftharpoons H_2COOH* + *$
$HCO* + H* \rightleftharpoons HCOH* + *$	$H_2COOH* + * \rightleftharpoons CH_2O* + OH*$
$HCOH* + H* \rightleftharpoons H_2COH* + *$	$CH_2O* + H* \rightleftharpoons CH_3O* + *$
$H_2COH* + H* \rightleftharpoons H_3COH* + *$	$CH_3O* + H* \rightleftharpoons H_3COH* + *$
$H_3COH* \rightleftharpoons CH_3OH + *$	

3.2.1. Kinetic Parameter

The kinetic parameters for each elementary step reaction should be determined to calculate the reaction rate. For each surface reaction, reaction rates are formulated by the following:

$$r_i = k_i \prod_j \theta_j = A_i \exp(-E_a/RT) \prod_j \theta_j \tag{6}$$

where k, A, and E_a are the kinetic parameters of the reaction i, the pre-exponential factor, and the activation energy, respectively. θ_j represents the portion of the surface intermediate j in the total catalytic active site over a catalytic surface. In the equation, the subscript j represents the reactants involved in the i-th reaction to comprise the terms of the driving forces, while the kinetic parameters were assumed to follow the Arrhenius type equation. The rate of the i-th elementary step (r_i) is expressed by the multiplication of the kinetic parameter and driving forces. Calculating A and E_a for each elementary step is one of the main problems in microkinetic modeling, and there are several different ways to obtain the parameters. When the computational chemistry is limited by poor computing power, the parameters are estimated by fitting experimental data. Due to its enhancement in computing capacity, computational chemistry is widely used, although it is still burdensome to calculate the parameters for a large amount of elementary steps. Accordingly, the BEP relations (also known as the linear free energy relations) [91,92] and the UBI-QEP method (also known as the bond-order conservation method) [93] are often used for more practical approaches. In 2011, Maestri and Reuter [94] proposed the refined UBI-QEP method, which could derive activation energies that have values similar to those derived from the DFT, as shown in Figure 11.
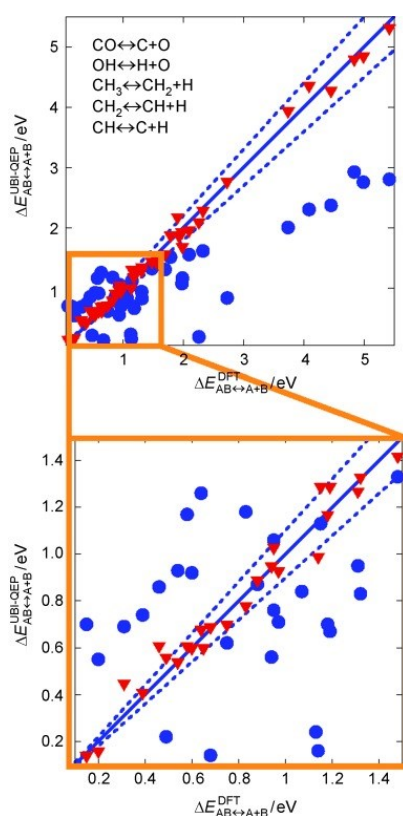

Figure 11. Parity plot of activation energies for several dissociation reactions on Rh(111) and Pt(111) as derived from the UBI-QEP and DFT (blue circle—original UBI-QEP; red triangle—refined UBI-QEP). Reprinted with permission from [94]. Copyright (2010) John Wiley and Sons.

3.2.2. Microkinetic Model

A microkinetic model is defined as a system of ordinary differential equations (ODEs) for the site balances:

$$\mathrm{d}\theta_j/\mathrm{d}t = \sum_i S_{ij}\, r_i \qquad (7)$$

where S_{ij} is the stoichiometric coefficient. For all surface intermediates, Equation (6), including the related elementary steps, is calculated simultaneously. By calculating the equations, the site fractions are obtained, and the consumption and production rates of gaseous species can be calculated through

the adsorption and desorption equations. Furthermore, the most abundant surface intermediate, dominant pathway, and rate-limiting steps can be elucidated as a result of the calculations. However, the kinetic parameters and reaction rates of different elementary steps have various orders of magnitude, making the ODE system so stiff that the calculation may become difficult. To reduce the stiffness, several solutions, such as scaling and the quasi-equilibrium assumption, have been adopted.

4. Conclusions

While there have been many microkinetic studies on MeOH synthesis since the 1990s, there were only a few on the microkinetic modeling of DME synthesis from MeOH. Many computational chemistry studies have been conducted since the DFT, and several quantum chemical methods were developed. From locating active sites to calculating reaction mechanisms, computational chemistry acts in an essential role.

In the past, computational chemistry was rarely used to develop microkinetic models. However, advances in computation performance accelerated computational chemistry-based microkinetic modeling. With the combination of computational chemistry and microkinetic analysis, researchers are now able to create a synergetic effect by analyzing reaction pathways both theoretically and kinetically. Moreover, kinetic parameters, such as pre-exponential factors and activation energies, can be obtained with theoretical backgrounds, and more elementary reactions can be considered. Many software programs (commercial and non-commercial), such as MATLAB®, Maple^{TM}, *kinsolv*, CHEMKIN, CatMAP, and the complex pathway simulator (COPASI), have been used for microkinetic studies of MeOH and DME synthesis.

The microkinetic modeling of MeOH and DME synthesis using computational chemistry was first conducted in the 2010s. Cu(111)- and Cu(211)-based CZA catalyst models have been mostly used because the surface of Cu(111) is known to be predominantly exposed and Cu(211) could represent the defective sites. For the rate-limiting step, the hydrogenation of methoxy intermediates or formic acid is suggested, while the dominant pathway between CO and CO_2 hydrogenation is still controversial. Several researchers have developed microkinetic models for MeOH synthesis on promising catalysts to replace CZA catalysts, with Pd-In catalysts being most actively studied (Table 3).

Still, there remains debate on whether the DME formation step via the dissociative pathway in DME synthesis is the rate-limiting step. Therefore, more studies on the microkinetic analysis of MeOH dehydration are necessary.

As the reaction mechanisms of MeOH and DME synthesis are not fully understood and new promising catalysts are continually being suggested, there is a need to accumulate more data by both computational chemistry and experimental studies. At the same time, the industrial application of microkinetic studies should be considered, which might require a multiscale modeling approach. Due to the complexity of microkinetic models, the direct augmentation of a microkinetic model in a reactor model using computational fluid dynamics (CFD) would almost be impossible. Therefore, a machine learning technique could be used to extract the information available in a microkinetic model, and then transfer it to a CFD reactor model in an implicative manner, thereby realizing a highly detailed level of the process simulation.

Author Contributions: Conceptualization, J.P. and H.S.K.; Data curation and draft preparation, J.P. and H.S.K.; Supervision, W.B.L. and M.-J.P.; Writing—review and editing, M.-J.P.; Formal analysis and investigation, W.B.L. and M.-J.P.; All authors have read and agreed to the published version of the manuscript.

References

1. Norskov, J.K.; Abild-Pedersen, F.; Studt, F.; Bligaard, T. Density functional theory in surface chemistry and catalysis. *Proc. Natl. Acad. Sci. USA* **2011**, *108*, 937–943. [CrossRef] [PubMed]
2. Van Speybroeck, V.; De Wispelaere, K.; Van Der Mynsbrugge, J.; Vandichel, M.; Hemelsoet, K.; Waroquier, M. First principle chemical kinetics in zeolites: The methanol-to-olefin process as a case study. *Chem. Soc. Rev.* **2014**, *43*, 7326–7357. [CrossRef] [PubMed]
3. Campbell, C.T. Future directions and industrial perspectives micro-and macro-kinetics: Their relationship in heterogeneous catalysis. *Top. Catal.* **1994**, *1*, 353–366. [CrossRef]
4. Bush, S.F.; Dyer, P. The experimental and computational determination of complex chemical kinetics mechanisms. *Proc. R. Soc. Lond. Ser. A* **1976**, *351*, 33–53.
5. Hickman, D.A.; Schmidt, L.D. Steps in CH4 oxidation on Pt and Rh surfaces: High-temperature reactor simulations. *AIChE J.* **1993**, *39*, 1164–1177. [CrossRef]
6. Oh, S.H.; Fisher, G.B.; Carpenter, J.E.; Goodman, D.W. Comparative kinetic studies of CO–O_2 and CO–NO reactions over single crystal and supported rhodium catalysts. *J. Catal.* **1986**, *100*, 360–376. [CrossRef]
7. Dumesic, J.A. *The Microkinetics of Heterogeneous Catalysis*; American Chemical Society: Washington, DC, USA, 1993; pp. 1–315.
8. Ali, K.A.; Abdullah, A.Z.; Mohamed, A.R. Recent development in catalytic technologies for methanol synthesis from renewable sources: A critical review. *Renew. Sustain. Energy Rev.* **2015**, *44*, 508–518. [CrossRef]
9. Ateka, A.; Pérez-Uriarte, P.; Gamero, M.; Ereña, J.; Aguayo, A.T.; Bilbao, J. A comparative thermodynamic study on the CO_2 conversion in the synthesis of methanol and of DME. *Energy* **2017**, *120*, 796–804. [CrossRef]
10. Olah, G.A.; Goeppert, A.; Prakash, G.K.S. Chemical recycling of carbon dioxide to methanol and dimethyl ether: From greenhouse gas to renewable, environmentally carbon neutral fuels and synthetic hydrocarbons. *J. Org. Chem.* **2009**, *74*, 487–498. [CrossRef]
11. Frusteri, F.; Bonura, G.; Cannilla, C.; Drago Ferrante, G.; Aloise, A.; Catizzone, E.; Migliori, M.; Giordano, G. Stepwise tuning of metal-oxide and acid sites of CuZnZr-MFI hybrid catalysts for the direct DME synthesis by CO_2 hydrogenation. *Appl. Catal. B Environ.* **2015**, *176*, 522–531. [CrossRef]
12. Centi, G.; Perathoner, S. Opportunities and prospects in the chemical recycling of carbon dioxide to fuels. *Catal. Today* **2009**, *148*, 191–205. [CrossRef]
13. Oloman, C.; Li, H. Electrochemical processing of carbon dioxide. *ChemSusChem* **2008**, *1*, 385–391. [CrossRef] [PubMed]
14. Li, H.; Oloman, C. Development of a continuous reactor for the electro-reduction of carbon dioxide to formate—Part 1: Process variables. *J. Appl. Electrochem.* **2006**, *36*, 1105. [CrossRef]
15. Li, H.; Oloman, C. Development of a continuous reactor for the electro-reduction of carbon dioxide to formate—Part 2: Scale-up. *J. Appl. Electrochem.* **2007**, *37*, 1107–1117. [CrossRef]
16. Lerner, A.; Brear, M.J.; Lacey, J.S.; Gordon, R.L.; Webley, P.A. Life cycle analysis (LCA) of low emission methanol and di-methyl ether (DME) derived from natural gas. *Fuel* **2018**, *220*, 871–878. [CrossRef]
17. Matzen, M.; Demirel, Y. Methanol and dimethyl ether from renewable hydrogen and carbon dioxide: Alternative fuels production and life-cycle assessment. *J. Clean. Prod.* **2016**, *139*, 1068–1077. [CrossRef]
18. Bae, C.; Kim, J. Alternative fuels for internal combustion engines. *Proc. Combust. Inst.* **2017**, *36*, 3389–3413. [CrossRef]
19. Chinchen, G.C.; Denny, P.J.; Parker, D.G.; Spencer, M.S.; Whan, D.A. Mechanism of methanol synthesis from CO_2/CO/H_2 mixtures over copper/zinc oxide/alumina catalysts: Use of 14C-labelled reactants. *Appl. Catal.* **1987**, *30*, 333–338. [CrossRef]
20. Grabow, L.C.; Mavrikakis, M. Mechanism of Methanol Synthesis on Cu through CO_2 and CO Hydrogenation. *ACS Catal.* **2011**, *1*, 365–384. [CrossRef]
21. Alharbi, W.; Kozhevnikova, E.F.; Kozhevnikov, I.V. Dehydration of Methanol to Dimethyl Ether over Heteropoly Acid Catalysts: The Relationship between Reaction Rate and Catalyst Acid Strength. *ACS Catal.* **2015**, *5*, 7168–7193. [CrossRef]
22. Din, I.U.; Shaharun, M.S.; Alotaibi, M.A.; Alharthi, A.I.; Naeem, A. Recent developments on heterogeneous catalytic CO_2 reduction to methanol. *J. CO2 Util.* **2019**, *34*, 20–33. [CrossRef]
23. Kakumoto, T. A theoretical study for the CO_2 hydrogenation mechanism on Cu/ZnO catalyst. *Energy Convers. Manag.* **1995**, *36*, 661–664. [CrossRef]

24. Kakumoto, T.; Watanabe, T. A theoretical study for methanol synthesis by CO_2 hydrogenation. *Catal. Today* **1997**, *36*, 39–44. [CrossRef]

25. Bauschlicher, C.W. A theoretical study of CO/Cu(100). *J. Chem. Phys.* **1994**, *101*, 3250–3254. [CrossRef]

26. Tameh, M.S.; Dearden, A.K.; Huang, C. Accuracy of Density Functional Theory for Predicting Kinetics of Methanol Synthesis from CO and CO_2 Hydrogenation on Copper. *J. Phys. Chem. C* **2018**, *122*, 17942–17953. [CrossRef]

27. Wellendorff, J.; Lundgaard, K.T.; Møgelhøj, A.; Petzold, V.; Landis, D.D.; Nørskov, J.K.; Bligaard, T.; Jacobsen, K.W. Density functionals for surface science: Exchange-correlation model development with Bayesian error estimation. *Phys. Rev. B* **2012**, *85*, 235149. [CrossRef]

28. Studt, F.; Abild-Pedersen, F.; Varley, J.B.; Nørskov, J.K. CO and CO_2 hydrogenation to methanol calculated using the BEEF-vdW functional. *Catal. Lett.* **2013**, *143*, 71–73. [CrossRef]

29. Reichenbach, T.; Mondal, K.; Jäger, M.; Vent-Schmidt, T.; Himmel, D.; Dybbert, V.; Bruix, A.; Krossing, I.; Walter, M.; Moseler, M. Ab initio study of CO_2 hydrogenation mechanisms on inverse ZnO/Cu catalysts. *J. Catal.* **2018**, *360*, 168–174. [CrossRef]

30. Behrens, M.; Studt, F.; Kasatkin, I.; Kühl, S.; Hävecker, M.; Abild-Pedersen, F.; Zander, S.; Girgsdies, F.; Kurr, P.; Kniep, B.L.; et al. The active site of methanol synthesis over $Cu/ZnO/Al_2O_3$ industrial catalysts. *Science* **2012**, *336*, 893–897. [CrossRef]

31. Van Den Berg, R.; Prieto, G.; Korpershoek, G.; Van Der Wal, L.I.; Van Bunningen, A.J.; Lægsgaard-Jørgensen, S.; De Jongh, P.E.; De Jong, K.P. Structure sensitivity of Cu and CuZn catalysts relevant to industrial methanol synthesis. *Nat. Commun.* **2016**, *7*, 1–7. [CrossRef]

32. Kattel, S.; Ramírez, P.J.; Chen, J.G.; Rodriguez, J.A.; Liu, P. Active sites for CO_2 hydrogenation to methanol on Cu/ZnO catalysts. *Science* **2017**, *355*, 1296–1299. [CrossRef] [PubMed]

33. Xu, D.; Wu, P.; Yang, B. Essential role of water in the autocatalysis behavior of methanol synthesis from CO_2 hydrogenation on Cu: A combined DFT and microkinetic modeling study. *J. Phys. Chem. C* **2019**, *123*, 5966–8959. [CrossRef]

34. Park, J.; Cho, J.; Lee, Y.; Park, M.J.; Lee, W.B. Practical microkinetic modeling approach for methanol synthesis from syngas over a Cu-based catalyst. *Ind. Eng. Chem. Res.* **2019**, *58*, 8663–8673. [CrossRef]

35. Huš, M.; Kopač, D.; Štefančič, N.S.; Jurković, D.L.; Dasireddy, V.D.B.C.; Likozar, B. Unravelling the mechanisms of CO_2 hydrogenation to methanol on Cu-based catalysts using first-principles multiscale modelling and experiments. *Catal. Sci. Technol.* **2017**, *7*, 5900–5913. [CrossRef]

36. Cheng, Z.; Lo, C.S. Mechanistic and microkinetic analysis of CO_2 hydrogenation on ceria. *Phys. Chem. Chem. Phys.* **2016**, *18*, 7987–7996. [CrossRef] [PubMed]

37. Sakahara, S.; Yajima, K.; Belosludov, R.; Takami, S.; Kubo, M.; Miyamoto, A. Combinatorial computational chemistry approach to the design of methanol synthesis catalyst. *Appl. Surf. Sci.* **2002**, *189*, 253–259. [CrossRef]

38. Baerlocher, C.; McCusker, L.B. Database of Zeolite Structures. Available online: http://www.iza-structure.org/databases/ (accessed on 25 May 2020).

39. Yarulina, I.; Chowdhury, A.D.; Meirer, F.; Weckhuysen, B.M.; Gascon, J. Recent trends and fundamental insights in the methanol-to-hydrocarbons process. *Nat. Catal.* **2018**, *1*, 398–411. [CrossRef]

40. Weckhuysen, B.M.; Yu, J. Recent advances in zeolite chemistry and catalysis. *Chem. Soc. Rev.* **2015**, *44*, 7022–7024. [CrossRef]

41. Haase, F.; Sauer, J. Interaction of Methanol with Brønsted Acid Sites of Zeolite Catalysts: An ab Initio Study. *J. Am. Chem. Soc.* **1995**, *117*, 3780–3789. [CrossRef]

42. Plessow, P.N.; Studt, F. Unraveling the Mechanism of the Initiation Reaction of the Methanol to Olefins Process Using ab Initio and DFT Calculations. *ACS Catal.* **2017**, *7*, 7987–7994. [CrossRef]

43. Waugh, K.C. Methanol synthesis. *Catal. Lett.* **2012**, *142*, 1153–1166. [CrossRef]

44. Medford, A.J.; Sehested, J.; Rossmeisl, J.; Chorkendorff, I.; Studt, F.; Nørskov, J.K.; Moses, P.G. Thermochemistry and micro-kinetic analysis of methanol synthesis on ZnO (0 0 0 1). *J. Catal.* **2014**, *309*, 397–407. [CrossRef]

45. Chinchen, G.C.; Denny, P.J.; Jennings, J.R.; Spencer, M.S.; Waugh, K.C. Synthesis of Methanol. Part 1. Catalysts and Kinetics. *Appl. Catal.* **1988**, *36*, 1–65. [CrossRef]

46. Taylor, P.A.; Rasmussen, P.B.; Ovesen, C.V.; Stoltze, P.; Chorkendorff, I. Formate synthesis on Cu(100). *Surf. Sci.* **1992**, *261*, 191–206. [CrossRef]

47. Askgaard, T.S.; Norskov, J.K.; Ovesen, C.V.; Stoltze, P. A Kinetic Model of Methanol Synthesis. *J. Catal.* **1995**, *156*, 229–242. [CrossRef]

48. Rasmussen, P.B.; Holmblad, P.M.; Askgaard, T.; Ovesen, C.V.; Stoltze, P.; Nørskov, J.K.; Chorkendorff, I. Methanol synthesis on Cu(100) from a binary gas mixture of CO_2 and H_2. *Catal. Lett.* **1994**, *26*, 373–381. [CrossRef]

49. Ovesen, C.V.; Clausen, B.S.; Schiøtz, J.; Stoltze, P.; Topsøe, H.; Nørskov, J.K. Kinetic implications of dynamical changes in catalyst morphology during methanol synthesis over Cu/ZnO catalysts. *J. Catal.* **1997**, *168*, 133–142. [CrossRef]

50. Clausen, B.S.; Schiøtz, J.; Gråbæk, L.; Ovesen, C.V.; Jacobsen, K.W.; Nørskov, J.K.; Topsøe, H. Wetting/ non-wetting phenomena during catalysis: Evidence from in situ on-line EXAFS studies of Cu-based catalysts. *Top. Catal.* **1994**, *1*, 367–376. [CrossRef]

51. Clausen, B.S.; Steffensen, G.; Fabius, B.; Villadsen, J.; Feidenhans'l, R.; Topsøe, H. In situ cell for combined XRD and on-line catalysis tests: Studies of Cu-based water gas shift and methanol catalysts. *J. Catal.* **1991**, *132*, 524–535. [CrossRef]

52. Clausen, B.S.; Gråbæk, L.; Steffensen, G.; Hansen, P.L.; Topsøe, H. A combined QEXAFS/XRD method for on-line, in situ studies of catalysts: Examples of dynamic measurements of Cu-based methanol catalysts. *Catal. Lett.* **1993**, *20*, 23–36. [CrossRef]

53. Gokhale, A.A.; Dumesic, J.A.; Mavrikakis, M. On the mechanism of low-temperature water gas shift reaction on copper. *J. Am. Chem. Soc.* **2008**, *130*, 1402–1414. [CrossRef] [PubMed]

54. Peter, M.; Fichtl, M.B.; Ruland, H.; Kaluza, S.; Muhler, M.; Hinrichsen, O. Detailed kinetic modeling of methanol synthesis over a ternary copper catalyst. *Chem. Eng. J.* **2012**, *203*, 480–491. [CrossRef]

55. Rubert-Nason, P.; Mavrikakis, M.; Maravelias, C.T.; Grabow, L.C.; Biegler, L.T. Advanced solution methods for microkinetic models of catalytic reactions: A methanol synthesis case study. *AIChE J.* **2014**, *60*, 1336–1346. [CrossRef]

56. Tang, Q.L.; Zou, W.T.; Huang, R.K.; Wang, Q.; Duan, X.X. Effect of the components' interface on the synthesis of methanol over Cu/ZnO from CO2/H2: A microkinetic analysis based on DFT + U calculations. *Phys. Chem. Chem. Phys.* **2015**, *17*, 7317–7333. [CrossRef] [PubMed]

57. Van Rensburg, W.J.; Petersen, M.A.; Datt, M.S.; Van Den Berg, J.A.; Van Helden, P. On the kinetic interpretation of DFT-derived energy profiles: Cu-catalyzed methanol synthesis. *Catal. Lett.* **2015**, *145*, 559–568. [CrossRef]

58. Van Helden, P.; Van Den Berg, J.A.; Weststrate, C.J. Hydrogen adsorption on co surfaces: A density functional theory and temperature programmed desorption study. *ACS Catal.* **2012**, *2*, 1097–1107. [CrossRef]

59. Medford, A.J.; Shi, C.; Hoffmann, M.J.; Lausche, A.C.; Fitzgibbon, S.R.; Bligaard, T.; Nørskov, J.K. CatMAP: A software package for descriptor-based microkinetic mapping of catalytic trends. *Catal. Lett.* **2015**, *145*, 794–807. [CrossRef]

60. Yang, N.; Medford, A.J.; Liu, X.; Studt, F.; Bligaard, T.; Bent, S.F.; Nørskov, J.K. Intrinsic selectivity and structure sensitivity of rhodium catalysts for C_{2+} oxygenate production. *J. Am. Chem. Soc.* **2016**, *138*, 3705–3714. [CrossRef]

61. Bonivardi, A.L.; Chiavassa, D.L.; Querini, C.A.; Baltanás, M.A. Enhancement of the catalytic performance to methanol synthesis from CO_2/H_2 by gallium addition to palladium/silica catalysts. In *Studies in Surface Science and Catalysis*; Elsevier: Amsterdam, The Netherlands, 2000; Volume 130, pp. 3747–3752.

62. Fujitani, T.; Nakamura, I. Methanol synthesis from CO and CO_2 hydrogenations over supported palladium catalysts. *Bull. Chem. Soc. Jpn.* **2002**, *75*, 1393–1398. [CrossRef]

63. Fujitani, T.; Saito, M.; Kanai, Y.; Watanabe, T.; Nakamura, J.; Uchijima, T. Development of an active Ga_2O_3 supported palladium catalyst for the synthesis of methanol from carbon dioxide and hydrogen. *Appl. Catal. A Gen.* **1995**, *125*, L199–L202. [CrossRef]

64. Chiavassa, D.L.; Collins, S.E.; Bonivardi, A.L.; Baltanás, M.A. Methanol synthesis from CO_2/H_2 using Ga_2O_3-Pd/silica catalysts: Kinetic modeling. *Chem. Eng. J.* **2009**, *150*, 204–212. [CrossRef]

65. Ye, J.; Liu, C.J.; Mei, D.; Ge, Q. Methanol synthesis from CO_2 hydrogenation over a Pd_4/In_2O_3 model catalyst: A combined DFT and kinetic study. *J. Catal.* **2014**, *317*, 44–53. [CrossRef]

66. Henkelman, G.; Uberuaga, B.P.; Jónsson, H. A climbing image nudged elastic band method for finding saddle points and minimum energy paths. *J. Chem. Phys.* **2000**, *113*, 9901–9904. [CrossRef]

67. Logadottir, A.; Rod, T.H.; Nørskov, J.K.; Hammer, B.; Dahl, S.; Jacobsen, C.J.H. The Brønsted-Evans-Polanyi relation and the volcano plot for ammonia synthesis over transition metal catalysts. *J. Catal.* **2001**, *197*, 229–231. [CrossRef]

68. Nørskov, J.K.; Bligaard, T.; Logadottir, A.; Bahn, S.; Hansen, L.B.; Bollinger, M.; Bengaard, H.; Hammer, B.; Sljivancanin, Z.; Mavrikakis, M.; et al. Universality in heterogeneous catalysis. *J. Catal.* **2002**, *209*, 275–278. [CrossRef]

69. Bligaard, T.; Nørskov, J.K.; Dahl, S.; Matthiesen, J.; Christensen, C.H.; Sehested, J. The Brønsted-Evans-Polanyi relation and the volcano curve in heterogeneous catalysis. *J. Catal.* **2004**, *224*, 206–217. [CrossRef]

70. Frei, M.S.; Capdevila-Cortada, M.; García-Muelas, R.; Mondelli, C.; López, N.; Stewart, J.A.; Curulla Ferré, D.; Pérez-Ramírez, J. Mechanism and microkinetics of methanol synthesis via CO_2 hydrogenation on indium oxide. *J. Catal.* **2018**, *361*, 313–321. [CrossRef]

71. Frei, M.S.; Mondelli, C.; García-Muelas, R.; Kley, K.S.; Puértolas, B.; López, N.; Safonova, O.V.; Stewart, J.A.; Curulla Ferré, D.; Pérez-Ramírez, J. Atomic-scale engineering of indium oxide promotion by palladium for methanol production via CO_2 hydrogenation. *Nat. Commun.* **2019**, *10*, 3377. [CrossRef]

72. García-Trenco, A.; Regoutz, A.; White, E.R.; Payne, D.J.; Shaffer, M.S.P.; Williams, C.K. PdIn intermetallic nanoparticles for the hydrogenation of CO_2 to methanol. *Appl. Catal. B Environ.* **2018**, *220*, 9–18. [CrossRef]

73. Wu, P.; Yang, B. Intermetallic PdIn catalyst for CO_2 hydrogenation to methanol: Mechanistic studies with a combined DFT and microkinetic modeling method. *Catal. Sci. Technol.* **2019**, *9*, 6102–6113. [CrossRef]

74. Carr, R.T.; Neurock, M.; Iglesia, E. Catalytic consequences of acid strength in the conversion of methanol to dimethyl ether. *J. Catal.* **2011**, *278*, 78–93. [CrossRef]

75. Moses, P.G.; Nørskov, J.K. Methanol to dimethyl ether over ZSM-22: A periodic density functional theory study. *ACS Catal.* **2013**, *3*, 735–745. [CrossRef]

76. Jones, A.J.; Iglesia, E. Kinetic, spectroscopic, and theoretical sssessment of sssociative and dissociative methanol dehydration routes in zeolites. *Angew. Chem. Int. Ed.* **2014**, *53*, 12177–12181. [CrossRef]

77. Lee, K.; Murray, É.D.; Kong, L.; Lundqvist, B.I.; Langreth, D.C. Higher-accuracy van der Waals density functional. *Phys. Rev. B* **2010**, *82*, 081101. [CrossRef]

78. Park, J.; Cho, J.; Park, M.J.; Lee, W.B. Microkinetic modeling of DME synthesis from methanol over H-zeolite catalyst: Associative vs. dissociative pathways. *Catal. Today* **2020**. [CrossRef]

79. Kohn, W.; Sham, L.J. Self-consistent equations including exchange and correlation effects. *Phys. Rev.* **1965**, *140*, A1133–A1138. [CrossRef]

80. Sabbe, M.K.; Reyniers, M.F.; Reuter, K. First-principles kinetic modeling in heterogeneous catalysis: An industrial perspective on best-practice, gaps and needs. *Catal. Sci. Technol.* **2012**, *2*, 2010–2024. [CrossRef]

81. Li, H.; Roy, P.N.; Le Roy, R.J. Analytic Morse/long-range potential energy surfaces and predicted infrared spectra for CO_2—H_2. *J. Chem. Phys.* **2010**, *132*, 214309. [CrossRef]

82. Feibelman, P.J.; Hammer, B.; Norskov, J.K.; Wagner, F.; Scheffler, M.; Stump, R.; Watwe, R.; Dumesic, J. The CO/Pt(111) puzzle. *J. Phys. Chem. B* **2001**, *105*, 4018–4025. [CrossRef]

83. Kresse, G.; Gil, A.; Sautet, P. Significance of single-electron energies for the description of CO on Pt(111). *Phys. Rev. B.* **2003**, *68*, 073401. [CrossRef]

84. Soini, T.M.; Genest, A.; Rösch, N. Assessment of hybrid density functionals for the adsorption of carbon monoxide on platinum model clusters. *J. Phys. Chem. A* **2015**, *119*, 4051–4056. [CrossRef] [PubMed]

85. Stroppa, A.; Termentzidis, K.; Paier, J.; Kresse, G.; Hafner, J. CO adsorption on metal surfaces: A hybrid functional study with plane-wave basis set. *Phys. Rev. B.* **2007**, *76*, 195440. [CrossRef]

86. Rohrbach, G.; Hafner, J.; Kresse, G. Molecular adsorption on the surface of strongly correlated transition-metal oxides: A case study for CO/NiO(100). *Phys. Rev. B.* **2004**, *69*, 075413. [CrossRef]

87. Schimka, L.; Harl, J.; Stroppa, A.; Grüneis, A.; Marsman, M.; Mittendorfer, F.; Kresse, G. Accurate surface and adsorption energies from many-body perturbation theory. *Nat. Mater.* **2010**, *9*, 741–744. [CrossRef]

88. Sheppard, D.; Terrell, R.; Henkelman, G. Optimization methods for finding minimum energy paths. *J. Chem. Phys.* **2008**, *128*, 134106. [CrossRef]

89. Raimondeau, S.; Vlachos, D.G. Recent developments on multiscale, hierarchical modeling of chemical reactors. *Chem. Eng. J.* **2002**, *90*, 3–12. [CrossRef]

90. Salciccioli, M.; Stamatakis, M.; Caratzoulas, S.; Vlachos, D.G. A review of multiscale modeling of metal-catalyzed reactions: Mechanism development for complexity and emergent behavior. *Chem. Eng. Sci.* **2011**, *66*, 4319–4355. [CrossRef]

91. Brönsted, J.N. Acid and basic catalysis. *Chem. Rev.* **1928**, *5*, 231–338. [CrossRef]

92. Evans, M.G.; Polanyi, M. Further considerations on the thermodynamics of chemical equilibria and reaction rates. *Trans. Faraday Soc.* **1936**, *32*, 1333–1360. [CrossRef]

93. Shustorovich, E.; Sellers, H. The UBI-QEP method: A practical theoretical approach to understanding chemistry on transition metal surfaces. *Surf. Sci. Rep.* **1998**, *31*, 1–119. [CrossRef]

94. Maestri, M.; Reuter, K. Semiempirical Rate Constants for Complex Chemical Kinetics: First-Principles Assessment and Rational Refinement. *Angew. Chem. Int. Ed.* **2011**, *50*, 1194–1197. [CrossRef] [PubMed]